Supplementary Information

Aggregation state transition strategy for fluorescence imaging of pyrethroid residues

Na Gu,[a] Yan Wang,[b] Zhengying Chen,[b] Hongke Bie,[a] Huili Wang,[a] Xuedong Wang [*a] and Chunyang Chen [*a, c]

[a.] *Jiangsu Key Laboratory of Environmental Science and Engineering, School of Environmental Science and Engineering, Suzhou University of Science and Technology, Suzhou 215009, P. R. China.*

[b.] *Suzhou Environmental Monitoring Center, Jiangsu Province, Suzhou 215129, P. R. China.*

[c.] *School of Chemistry and Chemical Engineering, Southeast University, Nanjing 210096, P. R. China.*

Corresponding Authors:

Chunyang Chen, Email: ccygroup@163.com

Xuedong Wang, Email: zjuwxd@163.com

The Supplementary Information contains 27 pages, including Figs. S1-S29 and Tables S1-S10.

Contents

1.Materials

m-Hydroxy diethylaniline, diethyl oxaloacetate (DEO), hydrochloric acid, 4-Diethylaminophenol(4-DEAP) ,7-diethylamino-4-ester coumarin（DEC4）, 7-diethylamino-3-ester coumarin(DEC3), sodium chloride, quinine sulfate, absolute ethanol, n-hexane, dichloromethane, 4-(diethylamino) salicylaldehyde（DEAS）,diethyl malonate, Phosphate Buffered Saline（PBS）, Hydrochloric Acid, acetic acid, piperidine, n-butanol, anhydrous sodium sulfate, petroleum ether, N,N-Dimethylformamide(DMF),Dimethyl Sulfoxide(DMSO), ethyl acetate, acetonitrile, and dioxane were all purchased from Adamas. zinc chloride, sodium chloride, sodium sulfate, anhydrous calcium chloride, anhydrous magnesium nitrate, anhydrous iron(III) chloride, copper(II) sulfate, aluminum chloride, sodium hydroxide,type II pyrethroids including deltamethrin (Del), fenvalerate (Fen), bifenthrin (Bif), cypermethrin (Cyp), cyfluthrin (Cyf), beta-cyfluthrin (BC), Permethrin (Per), lambda-cyhalothrin(Lam), organophosphorus pesticides like acephate (Ace), methamidophos (Map), methyl parathion(MP), and chlorpyrifos (Cpf), as well as amides and acetamiprid, methionine (Met), serine (Ser), leucine (Leu), histidine (His) and alanine (Ala) were purchased from Aladdin Corporation (Shanghai, China). All reagents were of analytical grade and used without further purification. Additionally, to ensure the quality of the experiment, the ultrapure water (>18.2 MΩ·cm) used in this experiment was produced by the Milli-Q system (Bedford, MA, USA).

2.Instruments

Table S1. List of instruments.

Instrument Name	Manufacturer
Nuclear Magnetic Resonance Spectroscopy	NMR, Bruker AVANCE III 400 MHz, Bruker, Switzerland
High-Resolution Mass Spectrometry	HRMS, Thermo Scientific Q Exactive Focus, USA
FTIR Spectroscopy（FT-IR）	Thermo Fisher Scientific, USA
FS5 Fluorescence Spectrometer	Edinburgh, UK
UV-5500PC UV-Vis Spectrophotometer	Kyoto, Japan
Steady-State/Transient Fluorescence Spectrometer	FLS1000，Edinburgh
Fluorescence Inverted Microscope	IX73, Japan
Zeta Potential Analyzer	DLS,Malvern Zetasizer Nano ZS90, UK
The Zebrafish Behavior Analysis Instrument	Danion Vision, Noldus, Netherlands
Electric Thermostatic Blast Drying Oven	Shanghai

3. Synthesis procedures

Synthesis of DEC3 (7-(Diethylamino)-3-(ethoxycarbonyl)coumarin):

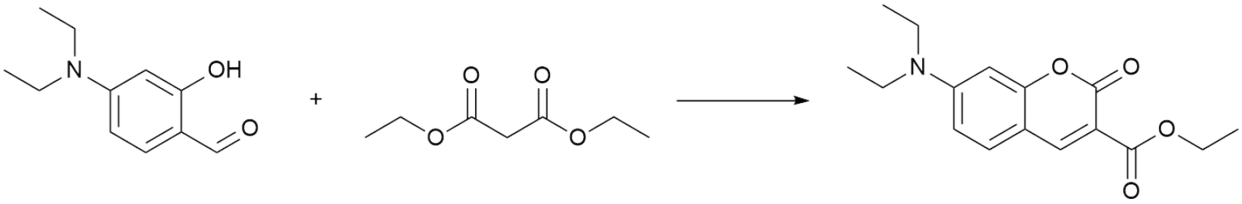

Scheme S1. Synthesis of DEC3.

To a 100 mL round-bottom flask equipped with a reflux condenser, 4-(diethylamino) salicylaldehyde (1.09 g, 5.58 mmol), diethyl malonate (795.50 µL, 5.24 mmol), and glacial acetic acid (140 mL) were added sequentially and stirred until complete dissolution. Piperidine (70 µL) was then introduced as a catalyst. n-Butanol (13.44 mL) was added as an azeotropic water-removal agent, and the reaction mixture was heated to 120 °C under oil

bath heating and stirred for 16 h. After cooling to room temperature, the reaction mixture was slowly poured into ice-water to quench the reaction. The resulting mixture was extracted with dichloromethane (3 × 100 mL). The combined organic phases were dried over anhydrous sodium sulfate and concentrated under reduced pressure at 40 °C using a rotary evaporator. The residue was recrystallized from a mixed solvent system of petroleum ether and n-hexane (v:v = 3:1), yielding orange-red crystals. The product was collected by vacuum filtration and dried under vacuum at 40 °C to afford DEC3 as a fluorescent greenish powder (Fig. S2) in 35% yield.

Synthesis of DEC4 (7-(Diethylamino)-4-(ethoxycarbonyl)coumarin):

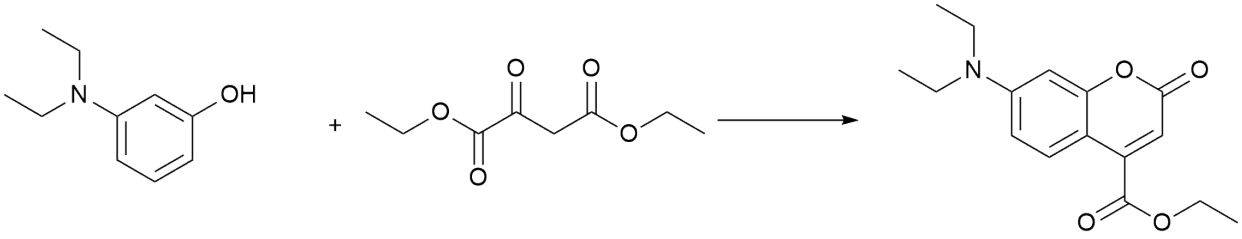

Scheme S2. Synthesis of DEC4.

To a round-bottom flask equipped with a reflux condenser, 3-diethylaminophenol (1.76 g, 10.0 mmol), diethyl oxaloacetate (2.70 g, 15.0 mmol), and anhydrous ethanol (30 mL) were added as solvent. A small piece of sodium ethoxide (~50 mg) was introduced as a base catalyst to promote the cyclization reaction. The reaction mixture was stirred under reflux at 80 °C for 96 h. Aliquots were sampled every 24 h and monitored by thin-layer chromatography (TLC) (eluent: n-hexane/CH_2Cl_2 = 1:2, v/v) to track reaction progress. Upon completion, the reaction mixture was cooled to room temperature and concentrated under reduced pressure using a rotary evaporator to afford the crude product. The crude material was adsorbed onto silica gel, dried, and purified by column chromatography. The column was packed and topped with n-hexane, and the compound was eluted with a mixture of n-hexane and dichloromethane (1:2, v/v). Fractions containing the desired product were combined based on TLC analysis, and the solvent was removed under reduced pressure to yield DEC4 as an orange-red powder (Fig. S1) in 31% yield.

4. Calculation of quantum yield

Via the relative method and compare with quinine sulfate at a wavelength of 360 nm, the quantum yield of quinine sulfate is 55%. The quantum yields of DEC4 and DEC3 at 420 nm and 424 nm were determined to be 47.57% and 16.25%, respectively. The relative quantum yield (RQY) is calculated using the following formula:

$$\Phi_X = \Phi_R \times \frac{A_R}{A_X} \times \frac{I_X}{I_R} \times \frac{\eta_X{}^2}{\eta_R{}^2}$$

Where Φ_X, A, I and η represent the quantum yield, integrated fluorescence intensity, absorbance value, and refractive index of the solution, respectively. R stands for quinine sulfate, and X represents the carbon dot solution.

5. Characterization of probes

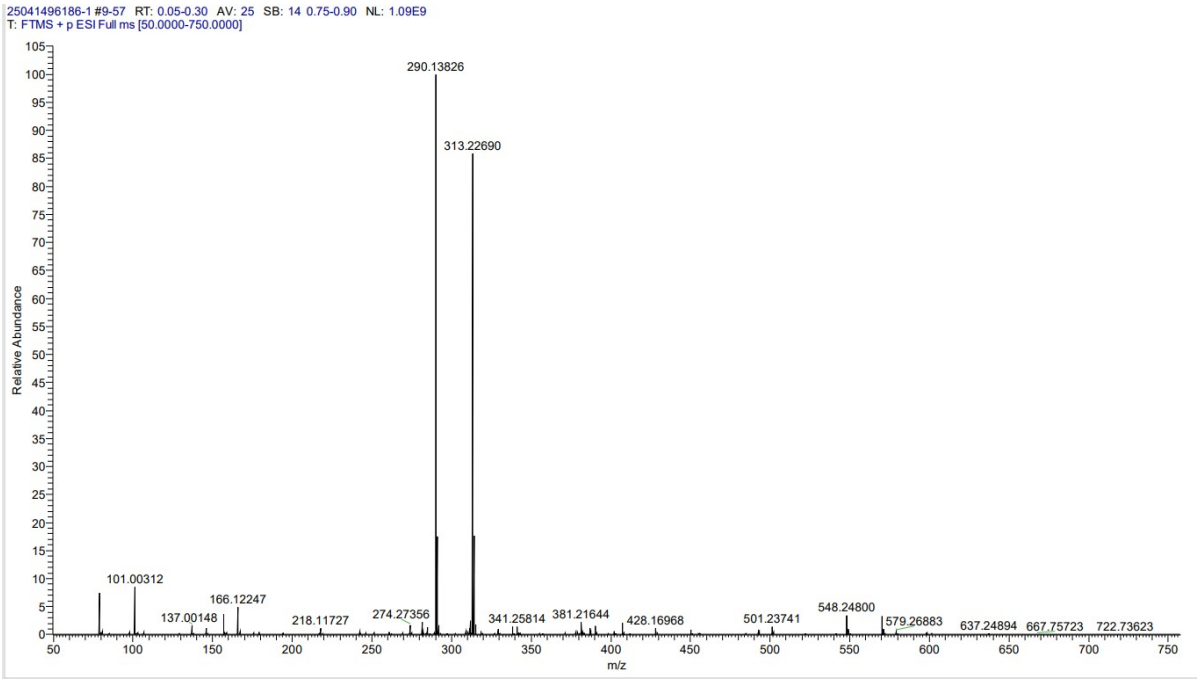

Fig. S1. High-resolution mass spectrometry positive spectrum of DEC4.

The molecular formula of DEC4 is $C_{16}H_{19}NO_4$. Its theoretical m/z for $[M+H]^+$ is 290.13923, which is in excellent agreement with the experimental value of 290.13826 shown in the spectrum.

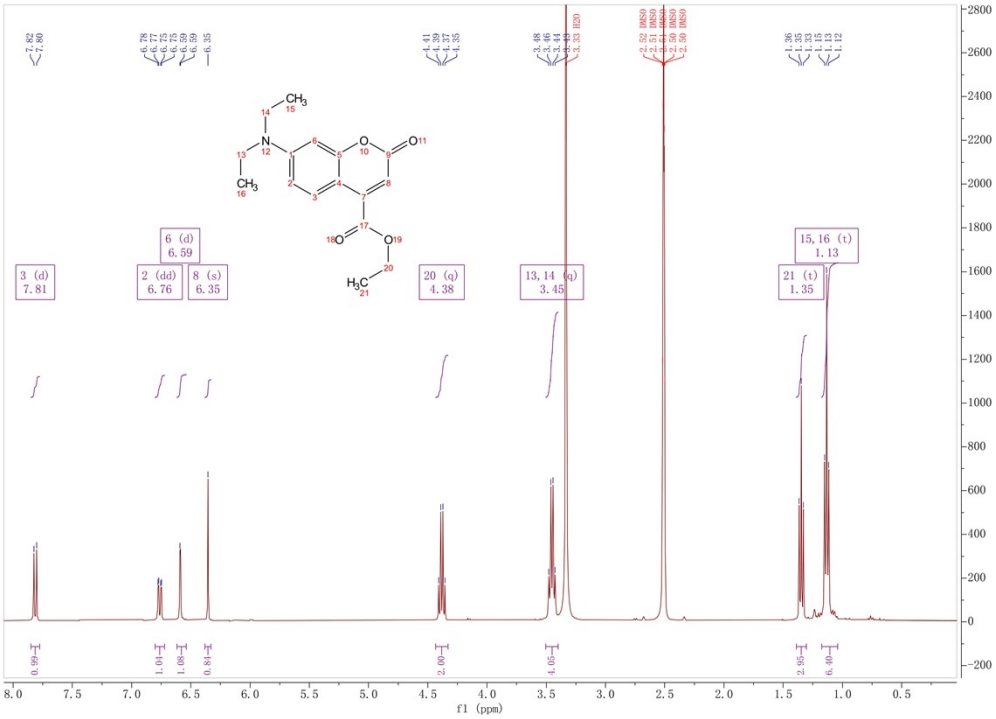

Fig. S2. ^{1}H NMR spectrum of DEC4.

^{1}H NMR (400 MHz, DMSO) δ 7.81 (d, *J* = 9.2 Hz, 1H), 6.76 (dd, *J* = 9.2, 2.6 Hz, 1H), 6.59 (d, *J* = 2.6 Hz, 1H), 6.35 (s, 1H), 4.38 (q, *J* = 7.1 Hz, 2H), 3.45 (q, *J* = 7.1 Hz, 4H), 1.35 (t, *J* = 7.1 Hz, 3H), 1.13 (t, *J* = 7.0 Hz, 6H).

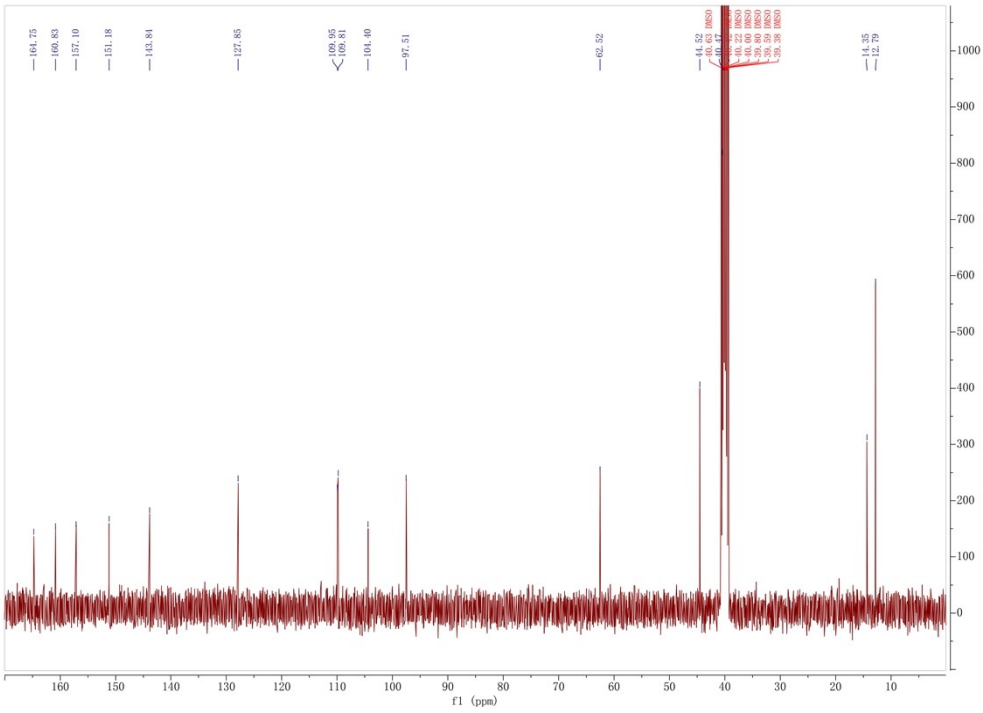

Fig. S3. ^{13}C NMR spectrum of DEC4.

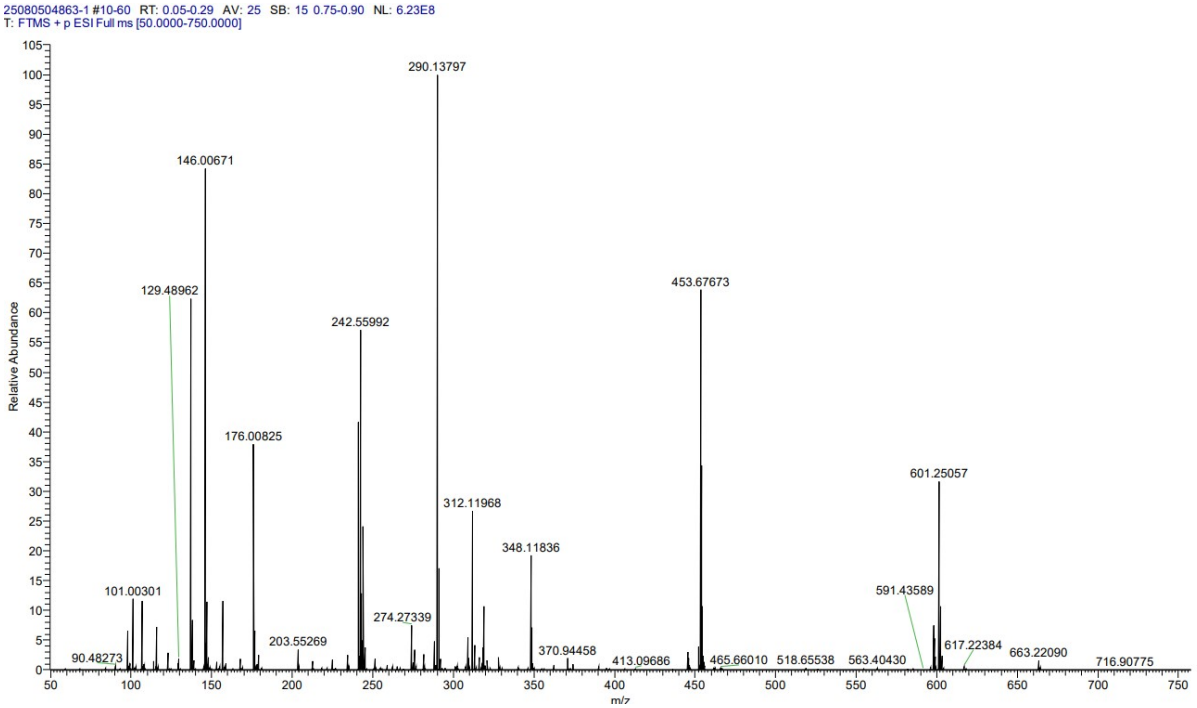

Fig. S4. High-resolution mass spectrometry positive spectrum of DEC3.

The molecular formula of DEC3 is $C_{16}H_{19}NO_4$. Its theoretical m/z for $[M+H]^+$ is 290.13923, which is in excellent agreement with the experimental value of 290.13797 shown in the spectrum.

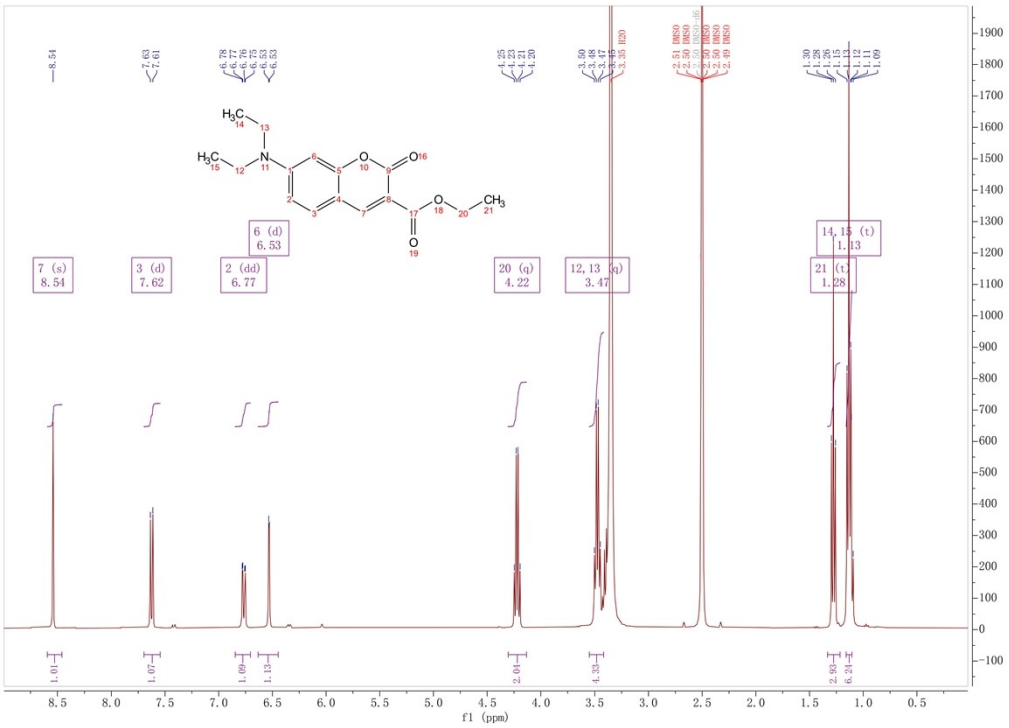

Fig. S5. ^{1}H NMR spectrum of DEC3.

^{1}H NMR (400 MHz, DMSO) δ 8.54 (s, 1H), 7.62 (d, *J* = 9.0 Hz, 1H), 6.77 (dd, *J* = 9.0, 2.4 Hz, 1H), 6.53 (d, *J* = 2.4 Hz, 1H), 4.22 (q, *J* = 7.1 Hz, 2H), 3.47 (q, *J* = 7.0 Hz, 4H), 1.28 (t, *J* = 7.1 Hz, 3H), 1.13 (t, *J* = 7.0 Hz, 6H).

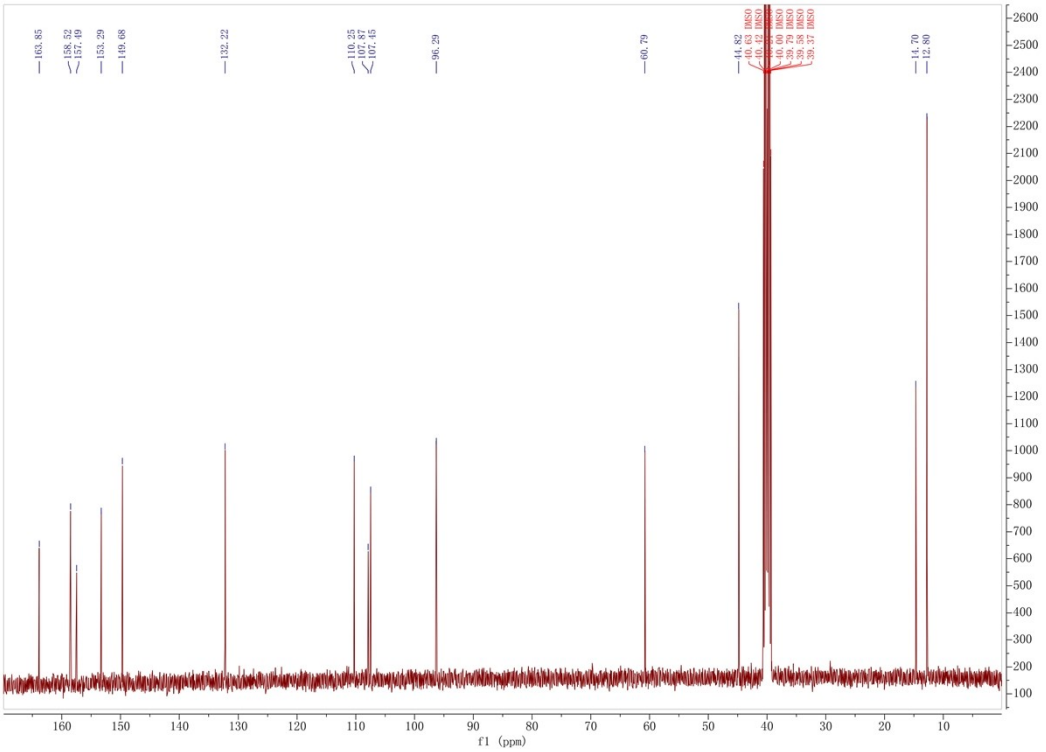

Fig. S6. ^{13}C NMR spectrum of DEC3.

6. Fluorescence detection methods

DEC4 stock solution (1 mM) was prepared by dissolving 0.28 mg of DEC4 in 1 mL of DMF, which can be stored at room temperature without light protection. For fluorescence experiments, 2 mL of ultrapure water and 2 μL of DEC4 solution were added to a cuvette, followed by 0-1.5 μL of a 10 mM pyrethroid standard solution (prepared in DMF). The mixture was vigorously stirred for 3 s, and fluorescence spectra were recorded from 430 to 650 nm using an excitation wavelength of 420 nm and a slit width of 3 nm. Eight pyrethroids (fenvalerate, Fen; deltamethrin, Del; lambda-cyhalothrin, LC; bifenthrin, Bif; cypermethrin, Cyp; cyfluthrin, Cyf; beta-cyfluthrin, BC; permethrin, Per) were tested for standard curve determination, while Fen was selected as the representative pyrethroid for all other tests. All tests were performed in triplicate unless otherwise specified. The same procedures were

repeated for DEC3. We systematically evaluated the effect of different DEC3 concentrations (ranging from 1 to 3 μM) on the detection of Fen (concentration range: 0 to 10.5 μM) to determine the optimal DEC3 concentration.

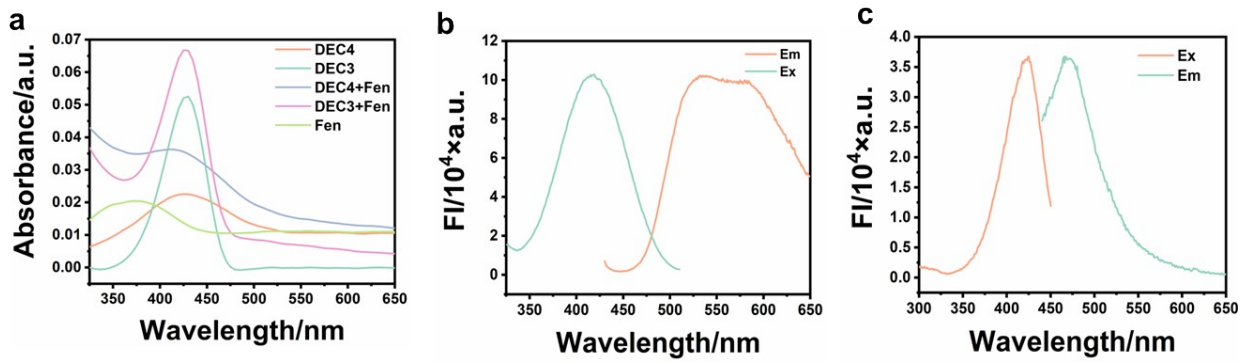

Fig. S7. (a) UV-Vis absorption spectra; excitation and emission spectra of DEC4 (b) and DEC3 (c).

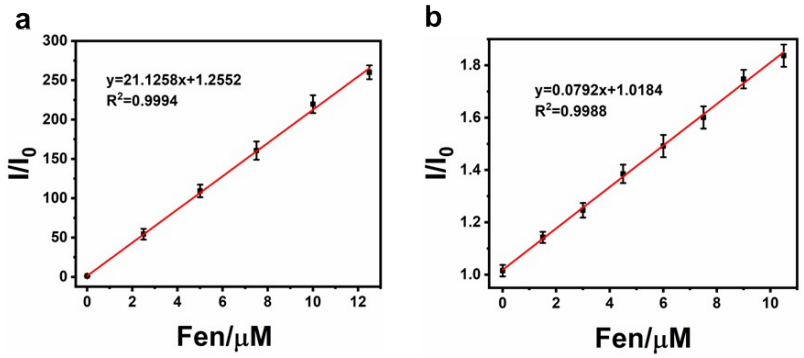

Fig. S8. Calibration curves of 1 mM DEC4 (a) and DEC3 (b) toward Fen.

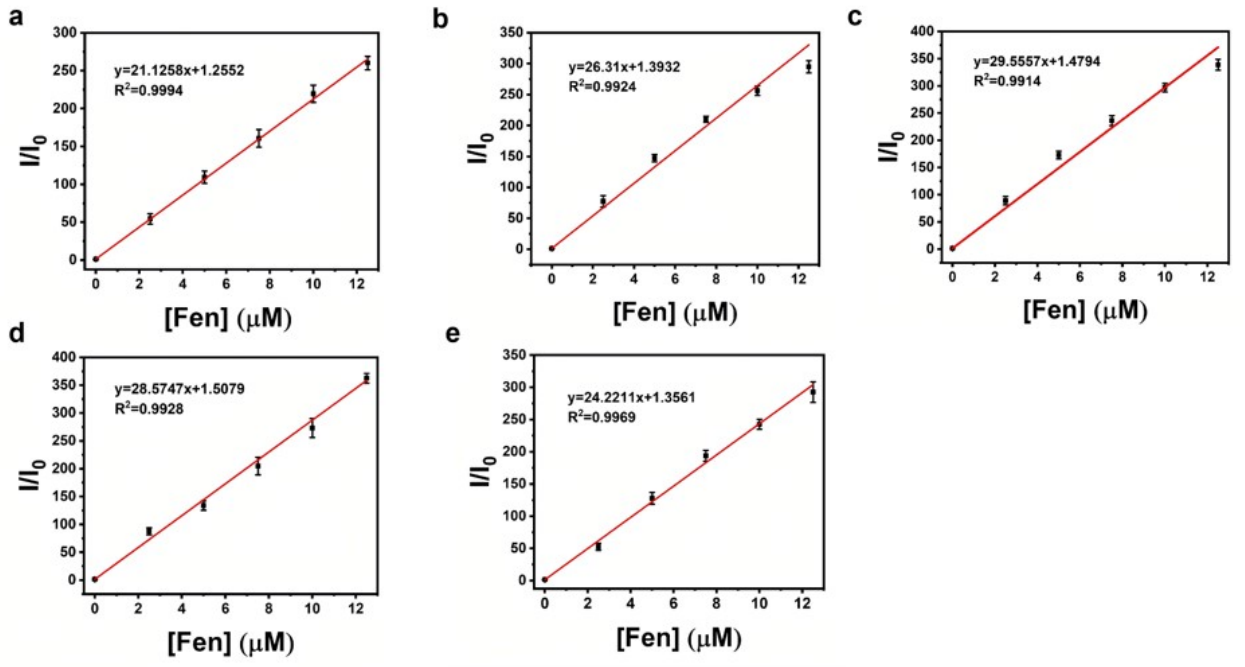

Fig. S9. Standard curves of 1 (a), (b), 3 (c), 4 (d) and 5 (e) μM DEC4 with Fen.

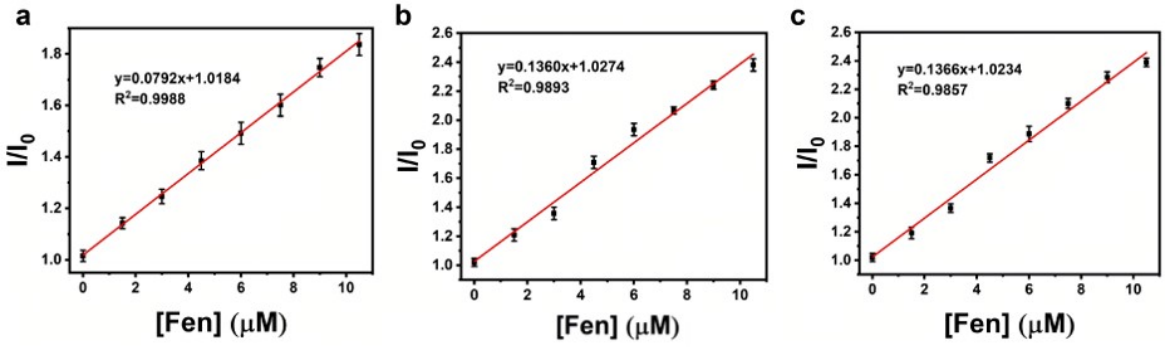

Fig. S10. Standard curves of 1 (a), 2 (b), 3 (c) μM DEC3 with Fen.

Table S2. LOD for different DEC4 concentration in Fen.

DEC4 (μM)	Linear equation	R^2	LOD (nM)
1.00	Y=21.1258X+1.2552	0.9994	0.27
2.00	Y=26.31X+1.3932	0.9924	0.22
3.00	Y=29.5557X+1.4794	0.9914	0.19
4.00	Y=28.5747X+1.5079	0.9928	0.20
5.00	Y=24.2211X+1.3561	0.9969	0.24

Table S3. LOD for different DEC3 concentration in Fen.

DEC4 (μM)	Linear equation	R^2	LOD (nM)
1.00	Y=0.0792X+1.0184	0.9988	0.27
2.00	Y=0.1360X+1.0274	0.9893	0.22
3.00	Y=0.1366X+1.0234	0.9857	0.24

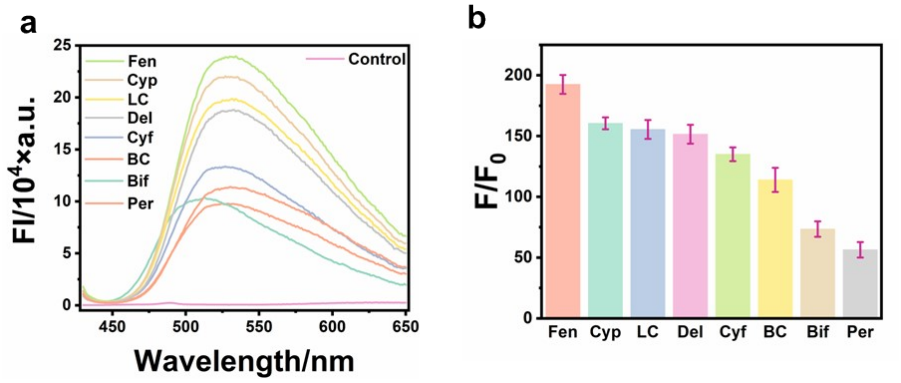

Fig. S11. (a) Fluorescence responses of DEC4 to various pyrethroids (7.50 μM); (b) fluorescence enhancement fold of DEC4 at 530 nm upon interaction with each pyrethroid.

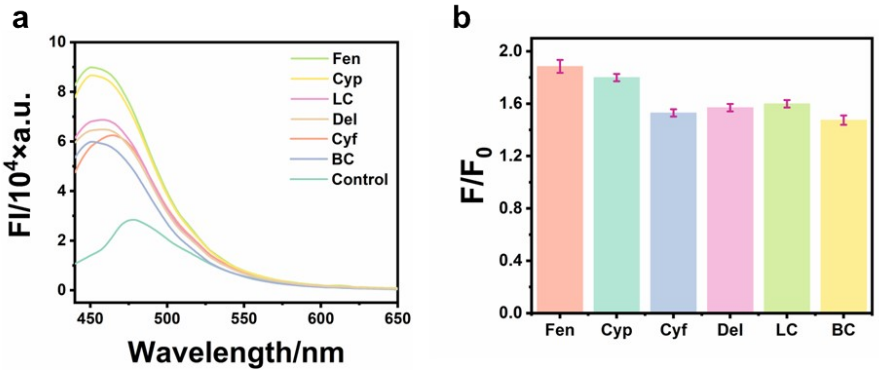

Fig. S12. (a) Fluorescence responses of DEC3 to various pyrethroids (10.50 μM); (b) fluorescence enhancement fold of DEC3 at 470 nm upon interaction with each pyrethroid.

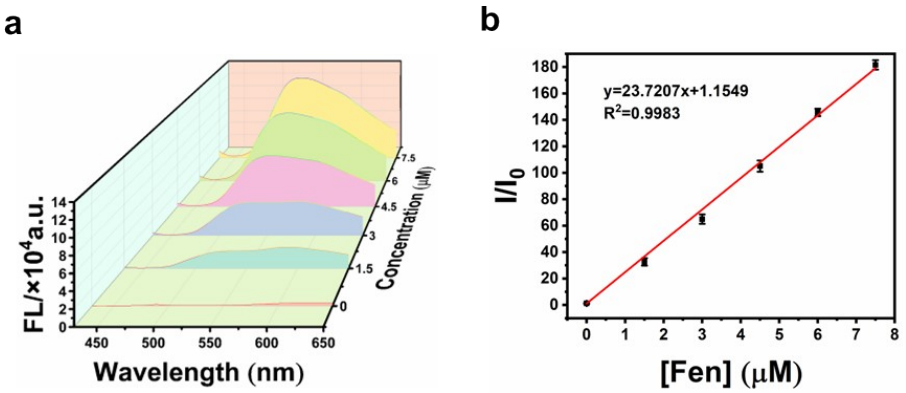

Fig. S13. Emission spectra (a) and calibration curve (b) of DEC4 (1 μM) upon addition of Fen.

First, 2 μL of 1 mM DEC3 was added to 2 ml of ultrapure water as a control solution. Subsequently, 4 μL aliquots of different pyrethroids (Lam, Cyp, Del, Cyf, BC, Fen, Bif, and Per) were individually added, and the fluorescence intensities were measured. During the investigation of the fluorescence response between DEC3 and Fen, varying concentrations of Fen (0-10.5 μM) were tested.

Table S4. LOD and LOQ of DEC4 for Pyrethroids.

Pyrethroids	Linear equation	LOD (nM)	LOQ (nM)
Fen	Y=23.7207X+1.1549	0.24	0.72
Cyf	Y=16.9742X+1.4042	0.34	1.01
Lam	Y=20.0091X+1.5954	0.29	0.85
Bif	Y=10.0730X+1.2526	0.57	1.70
Cyp	Y=20.3821X+1.3162	0.28	0.84
BC	Y=14.7621X+1.6962	0.39	1.16
Per	Y=6.0174X+1.0823	0.95	2.84
Del	Y=18.7107X+1.1929	0.30	0.91

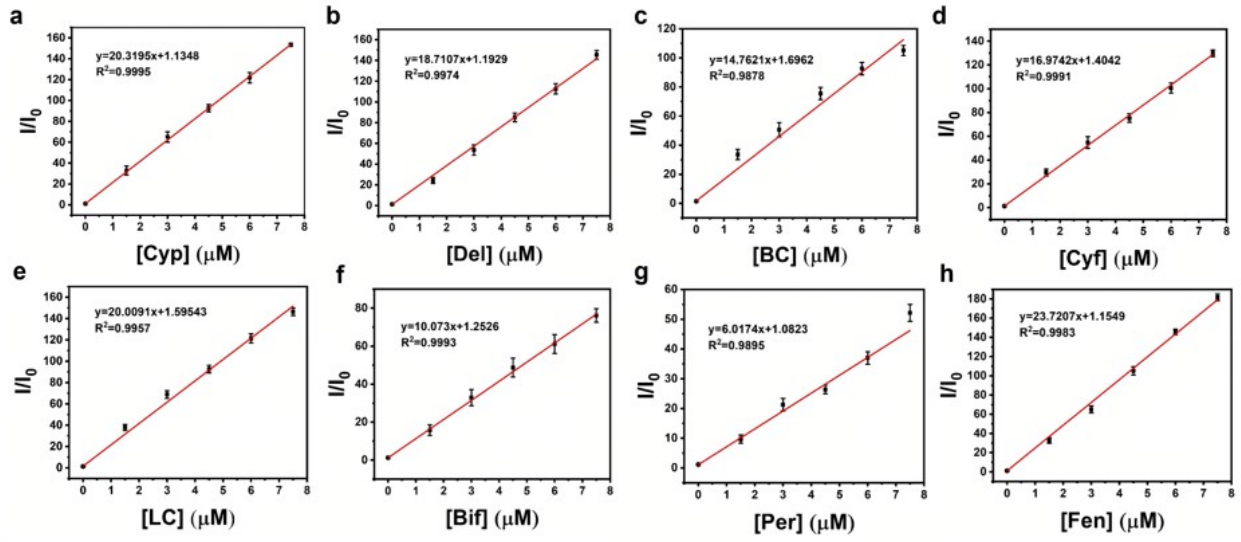

Fig. S14. Calibration curve of DEC4 (1 μM) upon addition of (a) Cyp, (b) Del, (c) BC, (d) Cyf, (e) LC, (f) Bif, (g) Per, (h) Fen.

Table S5. LOD and LOQ of DEC3 for Pyrethroids.

Pyrethroids	Linear equation	LOD (nM)	LOQ (nM)
Fen	Y=0.0792X+1.0184	71.97	215.91
Cyf	Y=0.0474X+1.0064	120.25	360.76
Lam	Y=0.0562X+1.0071	101.42	304.27
Cyp	Y=0.0723X+1.0101	78.84	236.51
BC	Y=0.0779X+1.0161	73.17	219.51
Del	Y=0.0781X+1.0118	72.98	218.95

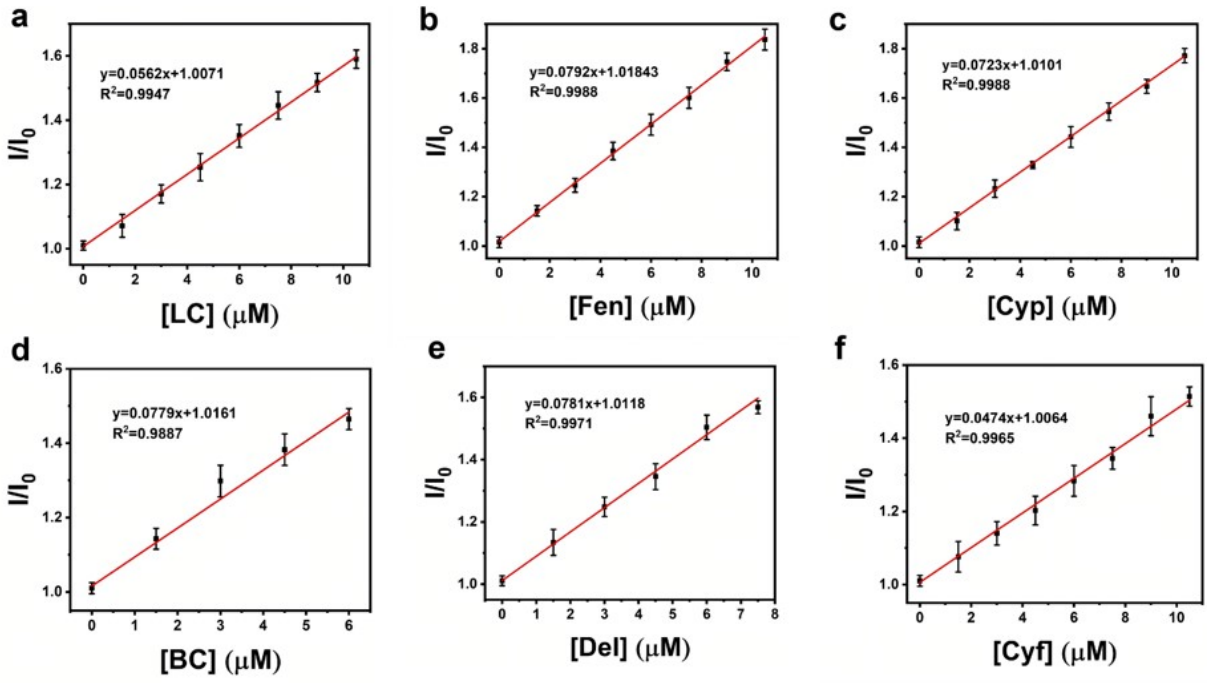

Fig. S15. Calibration curve of DEC3 (1 μM) upon addition of (a) LC, (b) Fen, (c) Cyp, (d) BC, (e) Del, (f) Cyf.

Table S6. Performance comparison between DEC4 and analogous detection methods.

Materials	Detection Targets	Linear range	LOD	Reaction time	References
AFL@ALB	Broad-spectrum	0-72 μM	1.0773 μM	10 s	[1]
NRF	Broad-spectrum	0.00-180.00 μg/L	1.50 μg/L	60 min	[2]
RCDs	LC	1-120 μg/L	0.89 μg/L	17 min	[3]
PNPs	LC	5-800 μg/L	0.034 μg/L	10 min	[4]
NCs@BSA	Cyp	0-180 μM	1.6432 μM	20 s	[5]
MIP-FeSe-QDs	Cyf	0.01-0.20 mg/L	1.3 μg/kg	5 min	[6]
DEC4	**Broad-spectrum**	**0.00-7.50 μM**	**0.24-0.95 nM**	**10 s**	**This work**

To assess the selectivity of the probe, potential interference was evaluated in the presence of Fen at its maximum detectable concentration (7.50 μM), and the interfering substances included inorganic ions (Ca^{2+}, Fe^{2+}, Fe^{3+}, Cu^{2+}, SO_4^{2-}, Mg^{2+}, Al^{3+}, K^{+}), natural amino acids (methionine, Met; serine, Ser; leucine, Leu; histidine, His; alanine, Ala), and representative pesticides (thiamethoxam, Tmx; acetamiprid, Ace; methyl parathion, MP; methamidophos, Map). Furthermore, to evaluate the anti-interference effects, each of the above-mentioned coexisting substances was added at an equal concentration to the 7.50 μM Fen solution, and the fluorescence emission spectra of DEC4 were recorded. Stability assessments were carried out under a variety of environmental conditions: temperatures (30, 40, and 50 °C), solvents (ultrapure water; DMF; dimethylsulfoxide, DMSO; ethyl acetate, EA; ethanol, EtOH; 1,4-dioxane, Diox), solution pH (0-12 in PBS), salt concentrations (0-0.6 M NaCl), storage durations (1, 3, 5, 7, and 14 days), and light exposure times (10, 30, 60, and 90 min under constant light intensity).

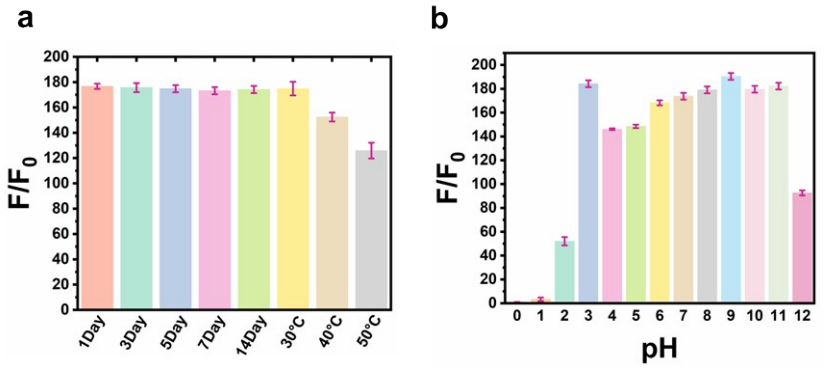

Fig. S16. Fluorescence response of DEC4 under the influence of storage time (a) and pH (b).

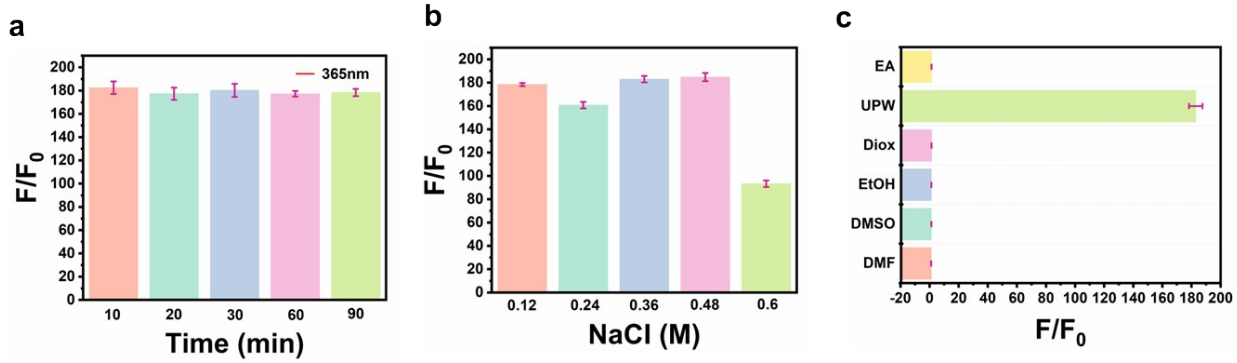

Fig. S17. Fluorescence response of DEC4 under the influence of light exposure time (a), salt concentration (b) and solvents (c).

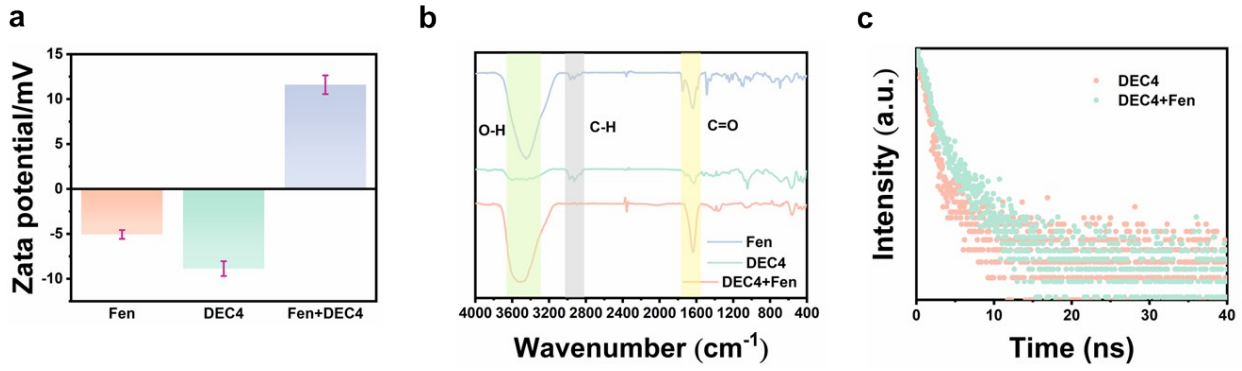

Fig. S18. Zeta potential (a), FTIR spectra (b) and fluorescence lifetime decay (c) of DEC4 before and after binding with Fen.

7. Mechanistic investigation

Initially, the stable molecular geometries were obtained via geometry optimization in Gaussian 16 at the B3LYP/6-311G level of theory. Subsequently, molecular docking was performed using AutoDock 1.5.7, where one DEC3/DEC4 molecule was defined as the macromolecule and another as the ligand to simulate self-aggregation. The resulting aggregate structures were then imported into Gaussian to calculate the corresponding excitation and emission data. Furthermore, using the DEC3/DEC4 in optimized aggregate as the docking template, the binding configurations and energetic variations between eight different pyrethroids and the DEC3/DEC4 were systematically investigated.

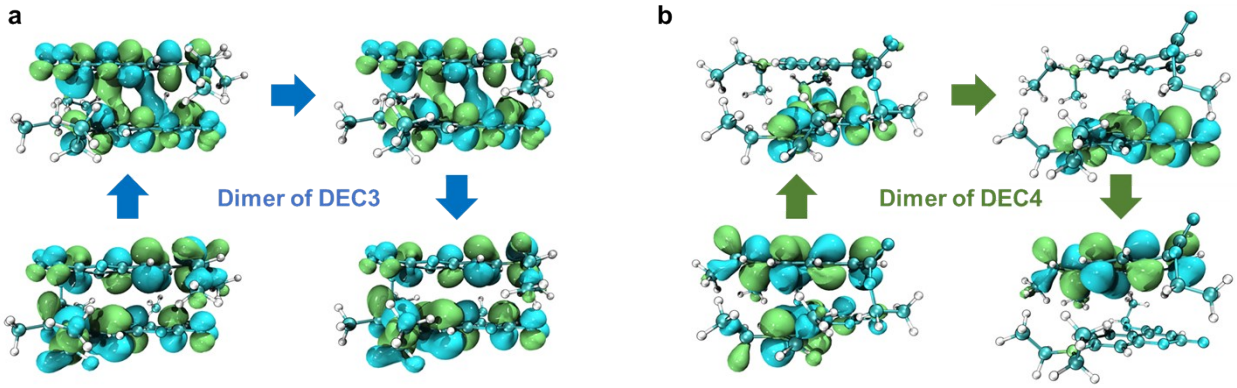

Fig. S19. Energy-level diagrams of frontier molecular orbitals involved in the excitation and emission processes of DEC3 (a) and DEC4 (b).

8. Detection methods for real samples

To simulate realistic pesticide deposition, Fen solutions in DMF at concentrations of 1.50, 3.00, 4.50, 5.50, 6.00, and 7.50 mM were uniformly sprayed onto the leaf surfaces of wheat plants. The samples were air-dried at room temperature for 2 h to mimic field drying conditions. Subsequently, residual extraction was performed by immersing samples in 10 mL of aqueous solution containing 1% (v/v) ACN. The resulting extracts were filtered through a 0.22-μm polyether sulfone membrane prior to analysis. To evaluate the accuracy of DEC4-based detection of Fen in samples, the extracts were quantitatively analyzed using HPLC coupled with a diode-array detector (HPLC-DAD). The operational conditions were as follows: a C18 reversed-phase column; injection volume of 20 μL; column temperature at 30 °C; mobile phase composed of ACN-water (70:30, v/v); flow rate of 1.0 mL/min; and detection wavelength set at 290 nm.

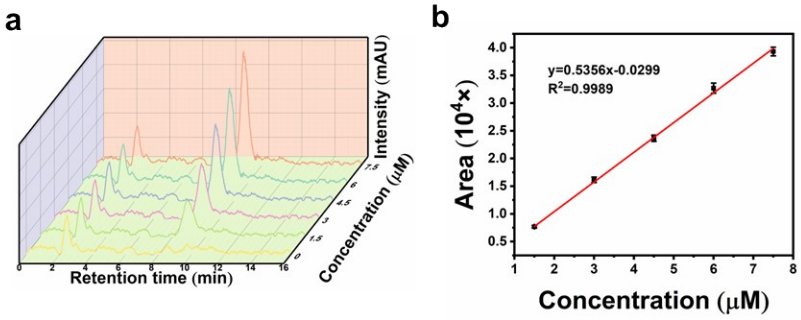

Fig. S20. (a) HPLC-DAD chromatogram of standard sample; (b) standard curve of absorption peak for standard sample.

Table S7. Extraction rate of Fen in wheat samples detected by HPLC-DAD.

Added Fen (μM)	Detected Fen (μM)	Extraction (%)	RSD (%)	Average extraction (%)
1.50	1.4342	95.61	1.45	95.30
	1.4163	94.42		
	1.3931	92.87		
3.00	2.8560	95.20	0.71	
	2.8158	93.86		
	2.8395	94.65		
4.50	4.2570	94.60	0.82	
	4.3254	96.12		
	4.2674	94.83		
6.00	5.7221	95.37	1.01	
	5.8320	97.20		
	5.8110	96.85		
7.50	7.1444	95.26	0.75	
	7.1933	95.91		
	7.2525	96.70		

Table S8. Recovery of Fen in wheat samples detected by fluorescence.

Added Fen (μM)	Detected Fen (μM)	Recovery (%)	RSD (%)	Average recovery (%)
	1.3917	92.78		
1.50	1.4159	94.39	1.42	
	1.4252	95.01		
	2.9229	97.43	1.96	
3.00	2.8236	94.12		
	2.8647	95.49		
	4.2867	95.26		
4.50	4.4177	98.17	1.82	95.98
	4.3268	96.15		
	5.8386	97.31		
6.00	5.8044	96.74	1.06	
	5.7312	95.52		
	7.2150	96.20		
7.50	7.2540	96.72	1.39	
	7.3808	98.41		

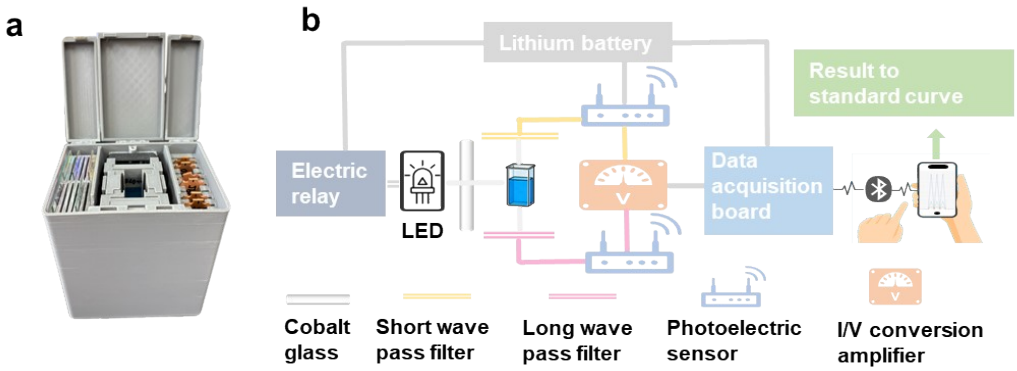

Fig. S21. Photograph (d) and schematic diagram (e) of FVT.

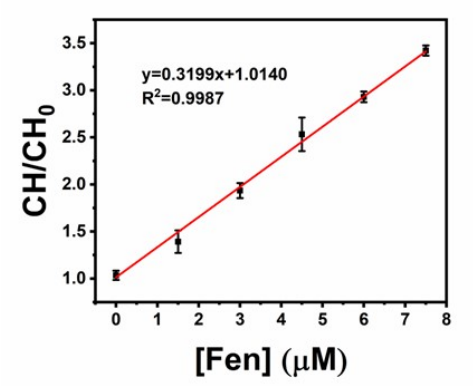

Fig. S22. FVT-based standard curve.

Table S9. Recovery of Fen in wheat samples detected by FVT Method.

Added Fen (μM)	Detected Fen (μM)	Recovery (%)	RSD (%)	Average recovery (%)
	1.4193	94.62		
1.50	1.4231	94.87	2.55	
	1.4751	98.34		
	2.9181	97.27		
3.00	2.8605	95.35	1.18	
	2.8947	96.49		
	4.3034	95.63		
4.50	4.4258	98.35	2.23	97.26
	4.5518	101.15		
	5.8092	96.82		
6.00	5.8434	97.39	1.07	
	5.7378	95.63		
	7.6380	101.84		
7.50	7.2188	96.25	3.28	
	7.4160	98.88		

Five-day-old wheat seedlings were randomly divided into two groups (n = 60 per group) to investigate the environmental fate of pesticide residues under different conditions. A 0.159 mM solution of Fen was uniformly sprayed onto the leaf surfaces of both groups, followed by a 15-day growth period. One group was maintained in a controlled indoor environment (sheltered from rain), while the other was exposed to outdoor conditions, including natural precipitation and ambient weather variations. To monitor the spatiotemporal dynamics of pyrethroid residues, the outermost fully expanded leaves were collected from each group every 24 h at a fixed time (15:00). Prior to imaging, the excised leaves were briefly immersed in a 0.1 mM aqueous solution of DEC4 for 1 s, quickly removed, and placed on clean glass slides. All samples were immediately imaged using an inverted fluorescence microscope equipped with a blue LED light source and a filter set to capture green fluorescence. The exposure time was standardized at 100 ms, and all other imaging parameters were kept constant to ensure comparability across samples.

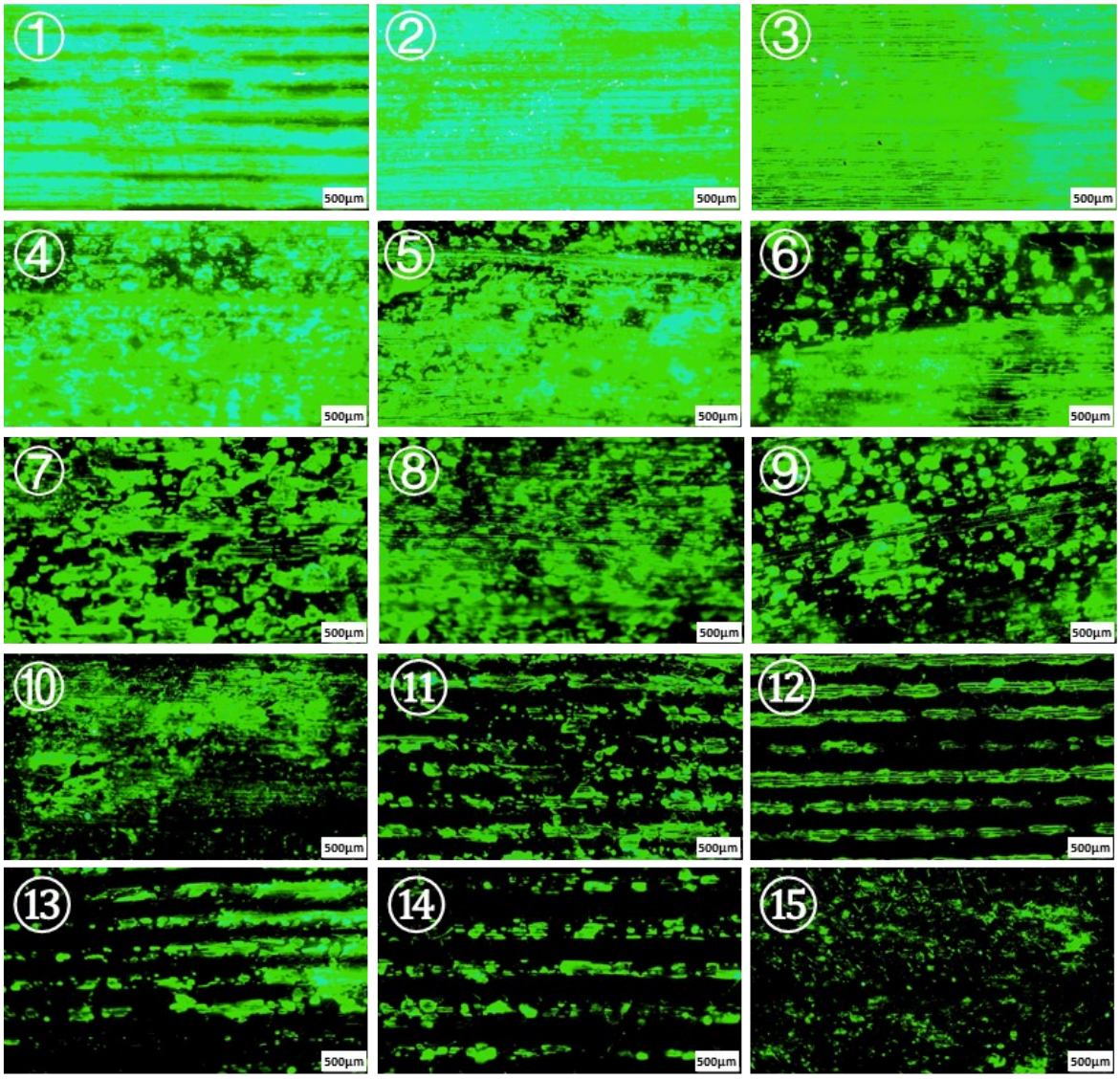

Fig. S23. Fluorescence imaging of Fen residues on outdoor-grown wheat leaf surfaces.

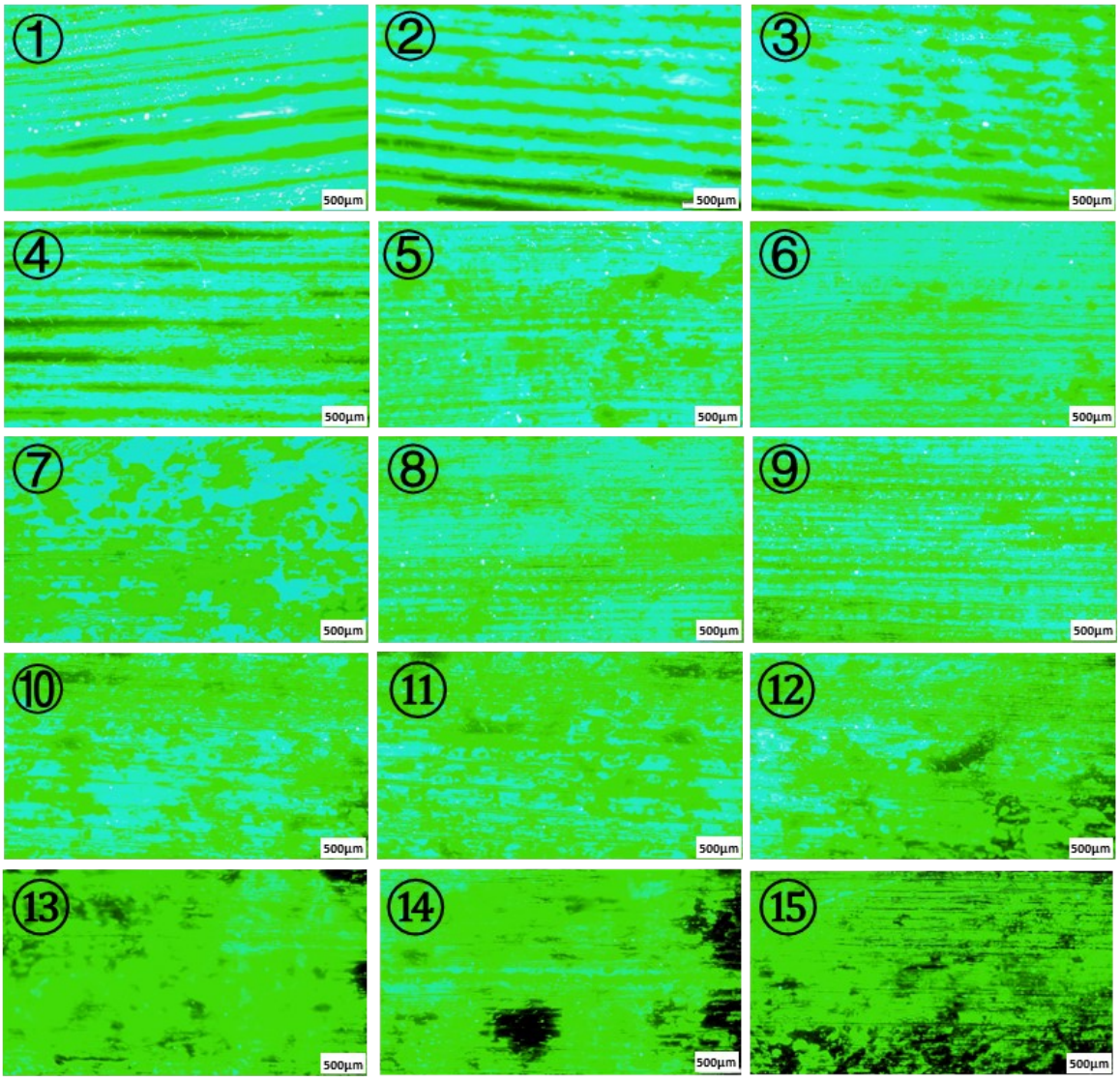

Fig. S24. Fluorescence imaging of Fen residues on indoor-grown wheat leaf surfaces.

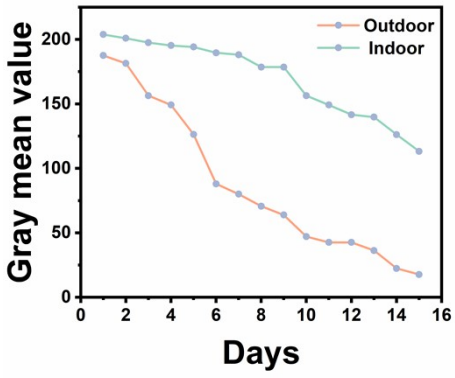

Fig. S25. Average grayscale value of fluorescence images.

Fluorescence images from the green channel were converted to grayscale, and the Mean Gray Value (MGV) of the entire image was calculated to represent the fluorescence intensity. As

images consisted exclusively of the leaf surface without background interference, the MGV accurately reflects the overall fluorescence dynamics within the target region.

9. Toxicologic study

To evaluate the potential environmental impact of waste solutions generated during the detection process, zebrafish (*Danio rerio*) embryos at 6 hours post-fertilization (hpf) were used as a model organism. Embryos were exposed in 24-well plates to either 1 μM DEC4 solution, 0.1 μM Fen solution, or a mixture of both solutions. After 120 hpf, the toxicity effects and environmental safety of the waste solutions were comprehensively assessed by observing behavioral changes, developmental abnormalities, and calculating the median lethal concentration (LC_{50}) in zebrafish embryos.

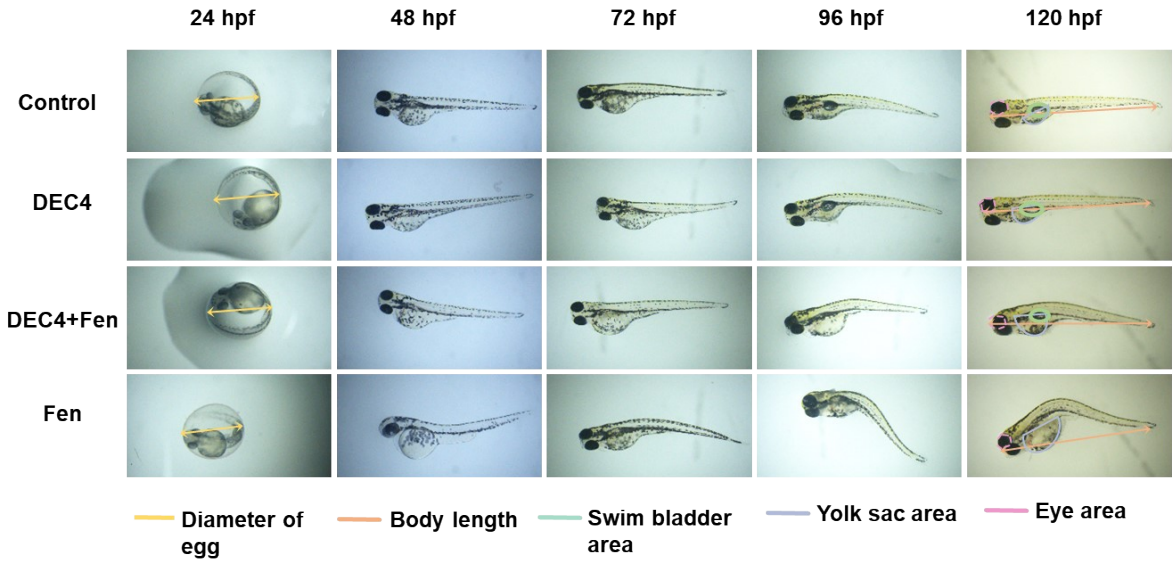

Fig. S26. Representative morphological features of zebrafish embryos from 24 to 120 hpf.

Table S10. Sizes of major organs in zebrafish (*Danio rerio*)

	Diameter of egg (mm)	Body length (mm)	Swim bladder area (mm^2)	Yolk sac area (mm^2)	Eye area (mm^2)
Control	347.09	922.73	5,992.9	19,600.0	4,417.4
DEC4	344.63	909.96	5,045.1	18,441.8	4,509.3
DEC4+Fen	323.73	863.42	2,880.0	16,322.4	4,135.7
Fen	322.84	821.24	/	15,318.1	3,999.8

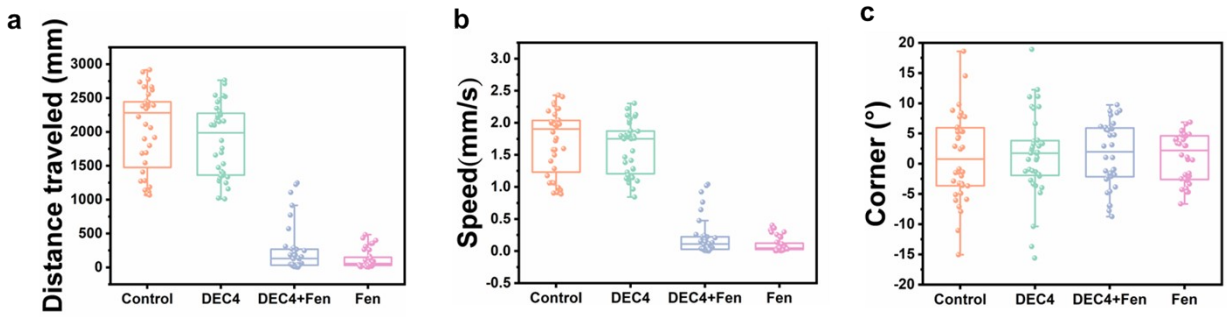

Fig. S27. Distance traveled (a), average swimming speed (b), and corner (c) of 120 hpf zebrafish.

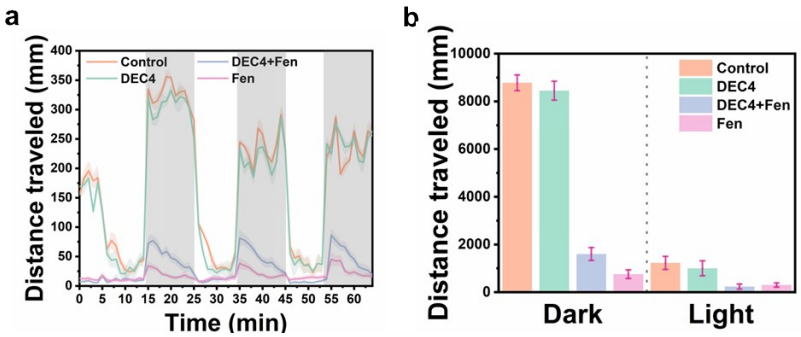

Fig. S28. Distance traveled (a) of zebrafish in response to light/dark transition stimuli, and total distance traveled (b) over the assay period.

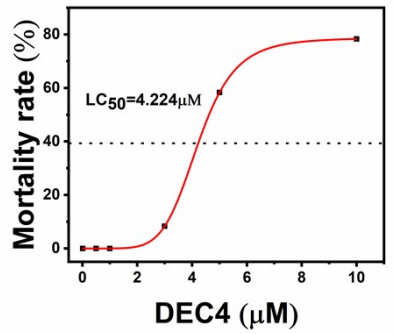

Fig. S29. LC_{50} of DEC4 in zebrafish at 120 hpf.

References

1 A. Liu, Q. Zhang, L. Pan, F. Yang, D. Lin and C. Jiang, *Anal. Chem.*, 2025, **97**, 13672-13680.

2 T. Jia, H. Tang, T. Qin, Y. Zhang, Y. Huang, Z. Xun, B. Liu, Z. Zhang, H. Xu and C. Zhao, *J. Agric. Food Chem.*, 2024, **72**, 3773-3782.

3 X. Zhu, X. Yuan, L. Han, H. Liu and B. Sun, *Biosens. Bioelectron.*, 2021, **191**, 113460.

4 X. Zhu, Q. Chuai, D. Zhang, H. Liu and B. Sun, *J. Agric. Food Chem.*, 2023, **71**, 3040-3049.

5 Z. Chen, J. Sun, G. Cheng, Y. Wang, H. Liu and H. Lin, *Microchem. J.*, 2025, **218**, 115443.

6 X. Li, H.-F. Jiao, X.-Z. Shi, A. Sun, X. Wang, J. Chai, D.-X. Li and J. Chen, *Biosens. Bioelectron.*, 2018, **99**, 268-273.